

Switchable large-gap quantum spin Hall state in two-dimensional MSi_2Z_4 materials class

Rajibul Islam,^{1,2,*} Rahul Verma,² Barun Ghosh,³ Zahir Muhammad,^{1,4}
Arun Bansil,³ Carmine Autieri,^{1,5,†} and Bahadur Singh^{2,‡}

¹*International Research Centre MagTop, Institute of Physics,
Polish Academy of Sciences, Aleja Lotników 32/46, PL-02668 Warsaw, Poland*

²*Department of Condensed Matter Physics and Materials Science,
Tata Institute of Fundamental Research, Colaba, Mumbai 400005, India*

³*Department of Physics, Northeastern University, Boston, Massachusetts 02115, USA*

⁴*Hefei Innovation Research Institute, School of Microelectronics, Beihang University, Hefei 230013, P. R. China*

⁵*Consiglio Nazionale delle Ricerche CNR-SPIN, UOS Salerno, I-84084 Fisciano (Salerno), Italy*

Quantum spin Hall (QSH) insulators exhibit spin-polarized conducting edge states that are topologically protected from backscattering and offer unique opportunities for addressing fundamental science questions and device applications. Finding viable materials that host such topological states, however, remains a challenge. Here by using in-depth first-principles theoretical modeling, we predict large bandgap QSH insulators in recently bottom-up synthesized two-dimensional (2D) MSi_2Z_4 ($M = \text{Mo}$ or W and $Z = \text{P}$ or As) materials family with $1T'$ structure. A structural distortion in the $2H$ phase drives a band inversion between the metal (Mo/W) d and p states of P/As to realize spinless Dirac cone states without spin-orbit coupling. When spin-orbit coupling is included, a hybridization gap as large as ~ 204 meV opens up at the band crossing points, realizing spin-polarized conducting edge states with nearly quantized spin Hall conductivity. We also show that the inverted band gap is tunable with a vertical electric field which drives a topological phase transition from the QSH to a trivial insulator with Rashba-like edge states. Our study identifies 2D MSi_2Z_4 materials family with $1T'$ structure as large bandgap, tunable QSH insulators with protected spin-polarized edge states and large spin-Hall conductivity.

Introduction:— Following the early studies of two-dimensional (2D) materials [1–4], Kane and Mele demonstrated the existence of a quantum spin Hall (QSH) state in graphene in the presence of symmetry-allowed spin-orbit coupling (SOC) [5, 6]. The QSH state features one-dimensional (1D) conducting helical edge modes inside an insulating bulk due to the nontrivial winding of their electronic states [5–12]. These helical edge modes carry symmetry-protected spin-polarized electronic states that hold immense potential to design high-efficiency quantum electronic devices with low dissipation [13–15]. The QSH state has been theoretically predicted in a variety of 2D materials and quantum well structures. However, the experimental realization of this state has so far been demonstrated only in HgTe/CdTe and InAs/GaSb quantum wells and thin-films of $1T'$ - WTe_2 , HgPt_2Se_3 , and Bi_4Br_4 at ultra-low temperatures [16–22]. A common approach to realize the QSH state is to reduce the thickness of three-dimensional (3D) Z_2 topological insulators to drive a 3D to 2D crossover and a band inversion in the surface states. This method has successfully predicted the QSH state in thin films of Z_2 topological insulators [11, 12, 23–26]. This approach for realizing the QSH state, however, remains challenging since it requires complex fine-tuning of either quantum well structure or film thickness to generate an inverted hybridization gap in the surface spectrum [11, 12, 23–29]. In the process, materials properties are often modified, leading to complicated electronic structures and quenching the quantized spin Hall conductance. Finding new strategies for

designing 2D materials with large inverted bandgaps to achieve the room temperature QSH state is thus highly desirable.

Here we present an in-depth first-principles analysis with optimized crystal structures to demonstrate the QSH state in recently introduced 2D materials that are realized via a bottom-up approach without parental analogues [30–32]. Such synthetic 2D materials provide a new paradigm for engineering designer states with diverse functionalities. Specifically, 2D MoSi_2N_4 materials were synthesized by passivating high-energy surfaces of non-layered nitrides with Si with remarkable stability under ambient conditions [32]. They show semiconducting behavior with high carrier mobility, and feature spin-valley locking, gating and thickness-tunable spin polarization, and 2D magnetism and correlation-driven quantum anomalous Hall state, among other properties depending on their compositions [33–36]. Theoretically predicted properties of these bottom-up synthesized materials are reported to be superior to those of the widely used 2D transition metal dichalcogenides (TMDs) [32, 33, 37, 38]. It is not clear, however, if these materials can form polytypic structures and realize the QSH state similar to the 2D TMDs. Here, based on our molecular dynamics simulations and phonon calculations, we predict that the $1T'$ phase of MSi_2Z_4 ($M = \text{Mo}$ or W , and $Z = \text{P}$ or As) is stable and realizes a QSH state via a structural distortion from $2H$ to $1T'$ phase. Our calculated inverted bandgap (~ 204 meV) and spin Hall conductivity (SHC) [$\sim 1.3e^2/h$] are found to be higher than

the top-to-bottom grown 2D TMDs. We also show that the QSH state of MSi_2Z_4 can be switched off by driving a topological phase transition via an applied (vertical) electric field. Our work indicates the robust presence of a switchable QSH state in a new polytypic structure of bottom-up grown 2D materials with excellent topological and spintronics properties.

Methods:— Electronic structure calculations were performed within the framework of density functional theory (DFT) based on the projector augmented wave method using the VASP [46, 47]. The self-consistent relativistic calculations were performed with a plane wave cut-off energy of 500 eV and a Γ centred $6 \times 12 \times 1$ k -mesh for Brillouin zone (BZ) sampling. We used the generalized gradient approximation (GGA) to include exchange-correlation effects [48]. The structural parameters were fully optimized until the residual forces on each atom were less than 0.001 eV/Å and the total energy is converged to 10^{-8} eV. For a more accurate treatment of electronic correlations, we also employed the Heyd-Scuseria-Ernzerhof (HSE) hybrid functional with 25% exact Hartree-Fock exchange [49]. Phonon dispersions were calculated with the density functional perturbation theory (DFPT) using the PHONOPY code [50] with a $2 \times 4 \times 1$ supercell. The *ab initio* molecular dynamics simulations were performed through the Nose-Hoover thermostat at a constant temperature of 300K with a time step of $2fs$ [51]. We generated material-specific tight-binding Hamiltonians with M d , Si s and p , and Z p orbitals using the VASP2WANNIER interface [52] which is ultimately used to elucidate topological properties using the Wanniertools package [53, 54].

Results:— The pristine phase of monolayer MSi_2Z_4 belongs to the 1H crystal structure family of 2D materials with space group D_{3h}^1 ($P6m2$, No. 187) [32, 33]. Figure 1(a) shows its crystal lattice with taking MoSi_2P_4 as an exemplar system. The structure is layered along the hexagonal c axis and can be viewed as a MoP_2 layer sandwiched between the two SiP layers, where the Mo atoms are located at the centre of the trigonal prism building block with six P atoms and the MoP_2 layer bonded vertically with the SiP layer [32]. In the $1T'$ phase of MoSi_2P_4 [Fig. 1(b)], the three atomic layers are locked in a way that the position of Mo atoms is at the centre of 60° twisted trigonal prism building block with six P atoms. This creates the octahedral local coordination of Mo atoms with the six P atoms in the MoP_2 layer but with different Mo-Mo bond lengths to form zig-zag atomic chains along the y axis and period-doubling along the x axis. Such a structural distortion lowers the hexagonal 1H symmetry to $1T'$ monoclinic symmetry with the space group $P2_1/m$ (No. 11) and forms a rectangular primitive unit cell as shown in Fig. 1(b). Importantly, the $1T'$ structure restores the inversion symmetry I in contrast to the 1H phase. Figure 1(c) illustrates the BZs associated with both the 1H and $1T'$ phases where high-

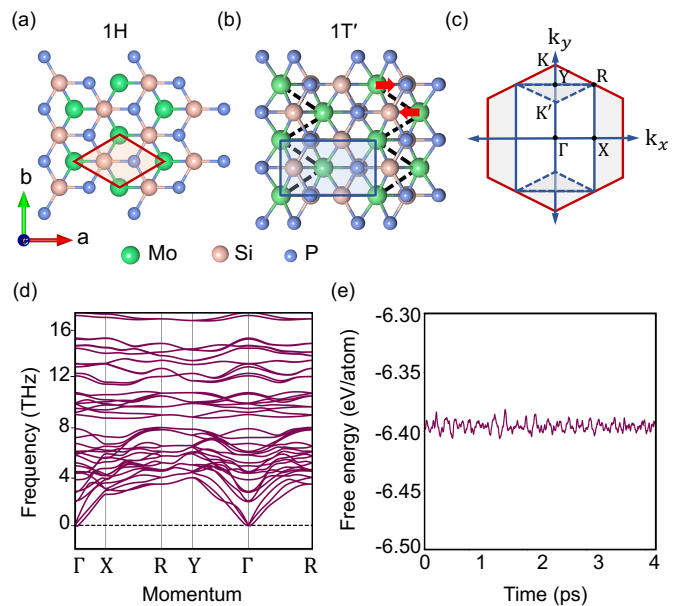


FIG. 1. Crystal structure of MoSi_2P_4 monolayer in (a) 1H and (b) $1T'$ phase. The unit cell of the 1H phase is indicated by the red rhombus in (a) and the $1T'$ phase is shown with the blue rectangle in (b). The Mo atoms are distorted from their original hexagonal positions to form 1D zigzag chains along the y axis in the $1T'$ phase as shown with dashed black lines in (b). (c) The associated 2D Brillouin zones (BZs) with high-symmetry points. The K points of the hexagonal BZ (red color) fold onto the $\Gamma - Y$ line of $1T'$ rectangular BZ (blue color). (d) Phonon dispersion in $1T'$ MoSi_2P_4 . (e) Total free energy of monolayer $1T'$ MoSi_2P_4 as a function of time step during the molecular dynamics simulation at $T = 300$ K.

symmetry points are marked in both the pristine hexagonal and reduced rectangular BZs.

To determine the stability of polytypic structures, we present the calculated phonon dispersion of monolayer $1T'$ of MoSi_2P_4 in Fig. 1(d). The absence of imaginary frequency modes throughout the BZ indicates the dynamical stability of the $1T'$ phase. The structural stability is further substantiated by performing *ab-initio* molecular dynamics simulations at 300 K. Variation of the free energy as a function of the simulation time is presented in Fig. 1(e). The energy oscillates near a mean value of 6.40 eV/atom. However, the monolayer structure remains intact at the end of the simulations without any new reconstruction of the lattice, indicating the thermal stability of the monolayer. We have also checked the thermodynamical stability of other members of the $1T'$ MSi_2Z_4 family and found them to be stable, see Supplemental Material (SM). Similar to structural stability and experimental realization of the $1T'$ phase of TMDs, these results elucidate that the $1T'$ - MSi_2Z_4 is stable and can be synthesized experimentally.

We now discuss the orbital-resolved electronic structures computed with GGA and HSE hybrid functionals

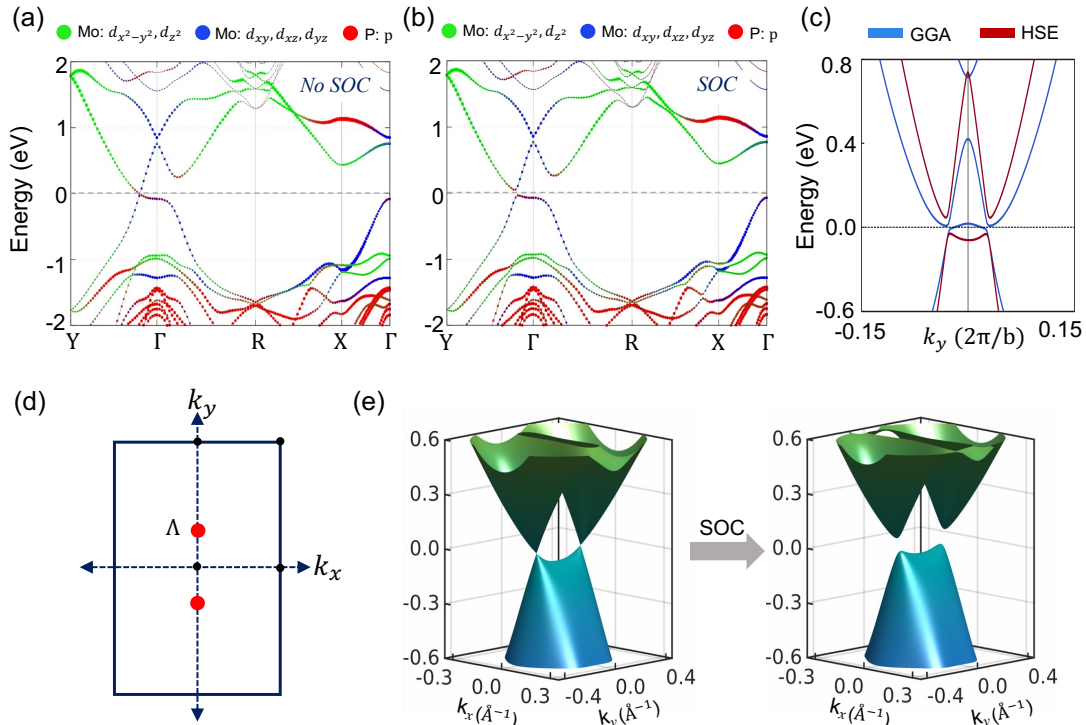


FIG. 2. Band structure of $1T'$ - MoSi_2P_4 (a) without and (b) with spin-orbit coupling using the HSE hybrid functional. The horizontal dashed line marks the Fermi level. The orbital compositions of bands are shown using different colors. (c) Closeup of bands obtained with HSE and GGA functionals along the $Y - \Gamma - Y$ line. (d) Location of valence and conduction band crossings at the Fermi level without spin-orbit coupling in the 2D Brillouin zone. (e) $E - k_x - k_y$ space rendition of spin-orbit-coupling-driven electronic structure crossover in monolayer $1T'$ - MoSi_2P_4 with the HSE functional.

TABLE I. Calculated structural and electronic parameters of 2D $1T'$ - MSi_2Z_4 ($M = \text{Mo}$ or W and $Z = \text{P}$ or As). The structural parameters include in-plane lattice constants a and b , and interatomic separation d_1 and d_2 in the transition-metal zigzag chain. The electronic parameters present the global band gap obtained with GGA (E_g^{GGA}) and HSE (E_g^{HSE}), the inverted bandgap at the Γ point calculated with GGA (δ^{GGA}) and HSE (δ^{HSE}). Summary of the topological state in 2D $1T'$ - MSi_2Z_4 is also given. QSH denotes quantum spin Hall state. See text for more details.

Material	a (\AA)	b (\AA)	d_1 (\AA)	d_2 (\AA)	Band gap (meV)		Inverted Gap (meV)		Topological invariant	Topological state
					E_g^{GGA}	E_g^{HSE}	δ^{GGA}	δ^{HSE}		
MoSi_2P_4	6.141	3.430	2.945	4.194	-10.4	86.2	398	842	$Z_2 = 1$	QSH
MoSi_2As_4	6.388	3.579	3.012	4.362	-39.5	109.2	391	800	$Z_2 = 1$	QSH
WSi_2P_4	6.129	3.441	2.939	4.133	-23.2	198.5	712	1079	$Z_2 = 1$	QSH
WSi_2As_4	6.364	3.589	2.993	4.368	-0.07	204.3	675	1058	$Z_2 = 1$	QSH

to delineate the topological state of various $1T'$ - MSi_2Z_4 compounds. Figures 2(a)-(b) show the representative HSE band structure of $1T'$ - MSi_2Z_4 taking MoSi_2P_4 as an example. The band structure is semimetallic with isolated spinless Dirac-type crossings on the $\Gamma - Y$ directions without SOC [Fig. 2(a)]. Adding relativistic effects to electronic structure opens a hybridization gap at these band crossings, thereby realizing a semiconducting state with a global bandgap E_g^{HSE} of 86 meV. The valence and conduction band extremum points are located away from time-reversal invariant momentum (TRIM) points at $\Lambda = \pm 0.103\text{\AA}^{-1}$ [red dots in 2(c)] on the $\Gamma - Y$

line, forming a camel-back-like band structure near the Γ point [39]. Such band structures generally imply a nontrivial topology. We find that the p states of P lie below the Mo d states with a clear band inversion at the Γ point, strong hybridization between the P and Mo states notwithstanding. This unusual orbital ordering is driven by a structural transition from $1H$ to $1T'$, which lowers the energy of the transition-metal states and results in a large inverted bandgap δ^{HSE} of 842 meV at the Γ point that is larger than the existing $1T'$ QSH materials. The calculated electronic and structural parameters of our investigated $1T'$ - MSi_2Z_4 materials are listed

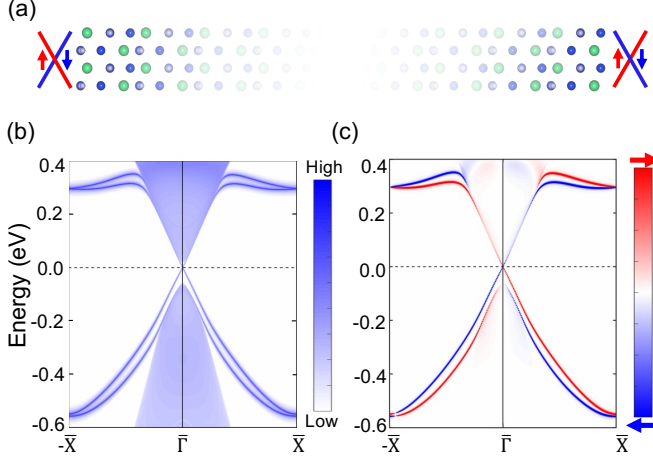


FIG. 3. (a) Lattice structure of semi-infinite one-dimensional edges of 1T'-MoSi₂P₄. Spin-polarized edge states are shown schematically on the left and right edges. (b) Electronic spectrum of (010) edge. Nontrivial edge states can be seen in the 2D bulk bandgap. (c) Calculated left-edge state spin-texture of 2D 1T'-MoSi₂P₄. Red and blue colors indicate the up and down spin polarization, respectively.

in Table I with band structures shown in the SM. Since monolayer 1T'-MSi₂Z₄ respects inversion symmetry, we calculated the Z_2 invariant from the parity eigenvalues of the occupied states at the TRIM points and found $Z_2 = 1$ (nontrivial) for all investigated materials. These results indicate that 2D 1T'-MSi₂Z₄ monolayers are QSH insulators.

We present the band structures obtained using HSE06 (red curves) and GGA (blue curves) along the Y-Γ-Y directions in Fig. 2(b) to estimate the bandgap corrections in 1T'-MSi₂Z₄ monolayers. The hybrid functionals are generally considered more accurate in estimating band bending, band order, and bandgap in comparison to the GGA functional. We find that while HSE06 corrects the inverted bandgap at the Γ point in comparison to GGA, the overall band structures obtained with the two functionals are topologically equivalent with a band inversion at the Γ point. Figure 2(d) presents the formation of QSH state in 1T'-MSi₂Z₄ monolayers by switching off the SOC. Specifically, the gapless band crossings are found at finite momenta along the Y-Γ-Y line at the Λ points. Switching on the SOC, hybridizes these band crossings to generate the QSH state. These results imply that the band inversion in 2D 1T'-MSi₂Z₄ emerges via the structural transition while the SOC is responsible for forming the QSH state.

The spin-polarized edge states protected by the time-reversal symmetry are the hallmark of the QSH state. To highlight these states, we plot the calculated edge spectrum and the associated spin-texture of MoSi₂P₄ in Fig. 3. Figure 3(a) depicts the terminated left and right edges along the y axis with schematics of the nontrivial

states of our xy monolayer (x remains the periodic direction). Since the two edges are related by inversion symmetry, we display states for the left edge in Figs. 3(b)-(c). A pair of counter-propagating states with opposite spin-polarization are seen inside the bandgap with a Dirac point at Γ . Similar results are found for other 1T'-MSi₂Z₄ materials.

Having established the QSH state in 1T'-MSi₂Z₄ monolayers, we now discuss their intrinsic spin Hall conductivity (SHC). We obtain the SHC σ_{xy}^z using the Kubo formula [40–44] as:

$$\sigma_{xy}^z = \frac{-e^2}{\hbar} \frac{1}{A} \sum_{\mathbf{k}} \Omega_{xy}^z(\mathbf{k}) \quad (1)$$

where,

$$\Omega_{xy}^z(\mathbf{k}) = \sum_n f_n(\mathbf{k}) \Omega_{n,xy}^z(\mathbf{k}) \quad (2)$$

is the k -resolved spin Berry curvature and

$$\Omega_{n,xy}^z(\mathbf{k}) = \hbar^2 \sum_{m \neq n} \frac{-2\text{Im}\langle n\mathbf{k} | \hat{J}_x^z | m\mathbf{k} \rangle \langle m\mathbf{k} | \hat{v}_y | n\mathbf{k} \rangle}{(E_{n\mathbf{k}} - E_{m\mathbf{k}})^2} \quad (3)$$

is the band resolved spin Berry curvature.

In Eqs. 1-3, A is the area of 2D unit cell and $|n\mathbf{k}\rangle$ denotes the Bloch state with energy $E_{n\mathbf{k}}$ and occupation $f_n(\mathbf{k})$. The spin current operator $\hat{J}_x^z = \frac{1}{2}\{\hat{\sigma}_z, \hat{v}_x\}$ with the spin operator $\hat{\sigma}_z$ and the velocity operator \hat{v}_x . The SHC $\sigma_{x,y}^z$ represents the spin-current along the x direction generated by the electric field along the y direction, and the spin current is polarized along the z direction. We consider a dense grid of 10^6 k -points in conjunction with maximally-localized Wannier functions to evaluate the spin Berry curvature and SHC. Figure 4(a) presents the calculated SHC as a function of the Fermi energy. The SHC is maximum near the band crossing points [marked with dashed line] reaching the highest value of $\sim 1.3 \frac{e^2}{h}$. The amplitude of SHC decreases quickly away from the band crossings points. This can be further seen from our band and k -resolved spin Berry curvature in Fig. 4(b). The spin Berry curvature is largely concentrated near the valence and conduction band-crossing point along the $\Gamma - Y$ direction having a SOC-driven hybridization gap. Notably, the perfect quantization of the SHC cannot be expected in QSH materials since they violate the S_z spin conservation [45]. However, MoSi₂P₄ shows a larger value of SHC than the other 1T' TMDs with the QSH state. An optimal setup to exploit the large SHC in MoSi₂P₄ should be in the clean limit with the Fermi level lying between the band crossings points.

We now demonstrate the tunability of the QSH state and the switching of the topological state under a vertical electric field. The topologically inverted bands between the transition metal d and pnictogen's p orbitals lie at

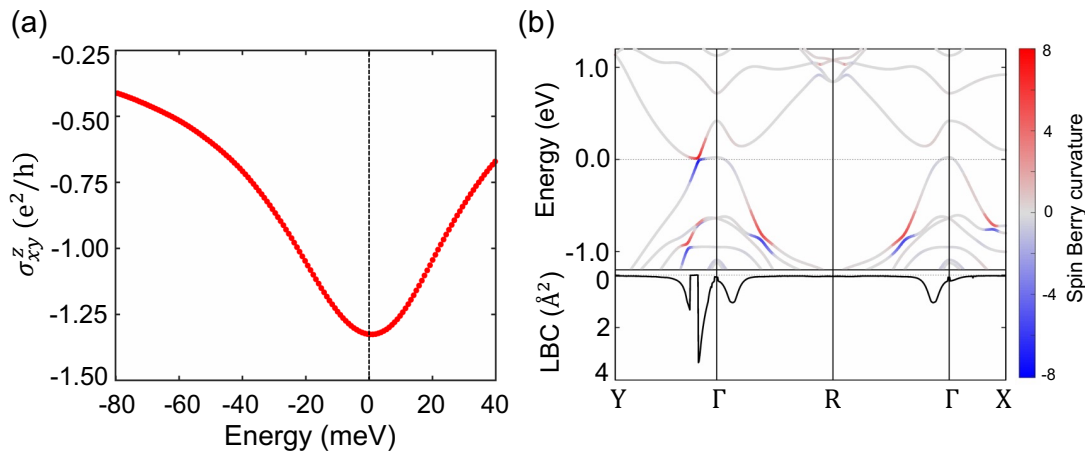


FIG. 4. (a) Intrinsic spin Hall conductivity (SHC) σ_{xy}^z as a function of Fermi energy for monolayer $1T'$ -MoSi₂P₄. SHC is given in units of $\frac{e^2}{h}$. Value of the SHC is maximum at the Fermi level. (b) Band-resolved (top) and k -resolved (bottom) spin Berry curvature of monolayer MoSi₂P₄ along the high-symmetry directions in the 2D Brillouin zone. LBC stands for logarithm of $\Omega_{xy}^z(\mathbf{k})$ (Eq. 2) and the colorbar refers to the logarithm of $\Omega_{n,xy}^z(\mathbf{k})$ (Eq. 3).

well-separated 2D planes in $1T'$ monolayer. This distinct spatial location of bands provides a natural basis for their tunability by an out-of-plane (vertical) electric field E_z . Figure 5 shows the HSE band structure for various electric field values. The electric field induces Rashba spin-splitting in the states by breaking inversion equivalence on the top and bottom sides of the mono-

layers. This is evident from spin-split states shown with distinct colors in the top row of Figs. 5(b)-(c). As the electric field increases, the band gap decreases to zero at the critical electric field value of $E_c = 0.187$ eV/Å where the spin-up and spin-down bands cross at the opposite Λ points. With further increase in the electric field, the bandgap reopens. An analysis based on the Z_2 invariants and edge-state dispersions (Fig. 5) shows that this bandgap closing drives a change in the topology to a trivial state with $Z_2 = 0$. This topological phase transition destroys the topological edge states thereby switching the QSH state in $1T'$ -MoSi₂P₄. A change in polarity of the electric field shows a similar topological phase transition to a trivial state. The evolution of QSH and trivial insulator state as a function of the applied electric field is displayed in Fig. 6.

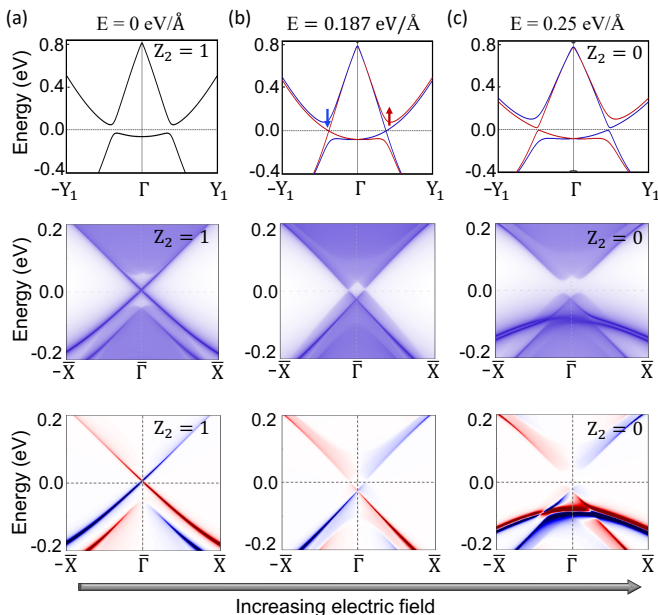


FIG. 5. Band structure of $1T'$ -MoSi₂P₄ monolayer for various values of the vertical electric field E_z : (a) 0, (b) 0.187, and (c) 0.250 eV/Å. The top, middle, and bottom rows show 2D band structure, (010) edge spectrum, and the edge-state spin-texture, respectively. Red and blue colors identify up and down spin states respectively.

The aforementioned results indicate an electric field on/off control of the spin-polarized edge currents in $1T'$ -MSi₂Z₄ in similar to the case of $1T'$ -TMDs [13]. Since the crystal symmetries of both these materials families are the same, various device ideas conceived for $1T'$ -TMDs can be applied to the MSi₂Z₄ family with the added advantage of a large inverted bandgap and large SHC. For example, monolayer MSi₂Z₄ could be interfaced with a large bandgap 2D insulator to protect the helical edge channels from being gapped by interlayer hybridization to realize a topological transistor [13]. When the Fermi level is placed in the nontrivial bandgap, a nearly quantized SHC would be realized in this device under zero or small electric fields. An electric field beyond the critical value of ± 0.187 eV/Å can switch off the quantized spin-Hall conductance, driving it into a trivial insulating state.

Summary:— We have demonstrated the existence of a tunable QSH state with a large bandgap in a new poly-

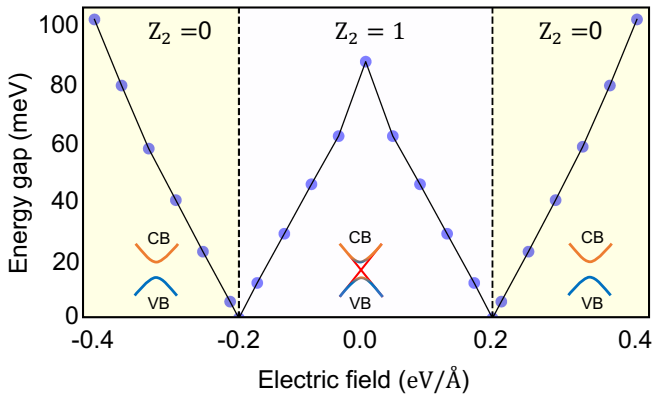


FIG. 6. Topological phase diagram of $1T'$ - MoSi_2P_4 as a function of the vertical electric field (E_z). Critical electric field strength for the topological phase transition from $Z_2 = 1$ to $Z_2 = 0$ state is marked with vertical dashed lines.

typic structure of the recently introduced bottom-up synthesized MSi_2Z_4 family of 2D materials. Our analysis based on phonon spectra and molecular dynamics simulations shows that these materials realize a thermodynamical stable $1T'$ phase in addition to the putative 1H phase. Our in-depth electronic structure modeling reveals that a structural distortion in the 1H phase leads to the $1T'$ structure and induces a topological band inversion. An inverted bandgap as large as 204 meV is found in the MSi_2Z_4 family that is even larger than in the existing $1T'$ -TMDs hosting a QSH ground state. Our calculated SHC shows a large value of $\sim 1.3 \frac{e^2}{h}$ in MoSi_2P_4 that arises from the large spin Berry curvature induced by spin-orbit-split bands at the band inversion points. We also show that the QSH state is tunable with a vertical electric field, which provides an external control for switching or turning on/off the QSH state. Our study thus not only introduces a new polytypic structure of recently introduced 2D MSi_2Z_4 materials, which supports a large bandgap QSH state, but it also shows that this new materials family will provide an excellent platform for realizing nontrivial states with large spin Hall conductance.

Acknowledgements:— This work is supported by the Department of Atomic Energy of the Government of India under project number 12-R&D-TFR-5.10-0100. The work at Institute of Physics, Polish Academy of Sciences is supported by the Foundation for Polish Science through the International Research Agendas program co-financed by the European Union within the Smart Growth Operational Programme and the National Science Center in the framework of the "PRELUDIUM" (Decision No.: DEC-2020/37/N/ST3/02338). We acknowledge the access to the computing facilities of the Interdisciplinary Center of Modeling at the University of Warsaw, Grant G84-0, GB84-1 and GB84-7. We ac-

knowledge the CINECA award under the ISCR initiative IsC93 "RATIO" and IsC99 "SILENTS" grant, for the availability of high-performance computing resources and support. The work at Northeastern University was supported by the Air Force Office of Scientific Research under award number FA9550-20-1-0322, and benefited from the computational resources of Northeastern University's Advanced Scientific Computation Center (ASCC) and the Discovery Cluster.

* rislam@magtop.ifpan.edu.pl

† autieri@magtop.ifpan.edu.pl

‡ bahadur.singh@tifr.res.in

- [1] K. S. Novoselov, "Nobel lecture: Graphene: Materials in the flatland," *Rev. Mod. Phys.* **83**, 837–849 (2011).
- [2] A. H. Castro Neto, F. Guinea, N. M. R. Peres, K. S. Novoselov, and A. K. Geim, "The electronic properties of graphene," *Rev. Mod. Phys.* **81**, 109–162 (2009).
- [3] K. S. Novoselov, D. Jiang, F. Schedin, T. J. Booth, V. V. Khotkevich, S. V. Morozov, and A. K. Geim, "Two-dimensional atomic crystals," *Proc. Natl. Acad. Sci.* **102**, 10451–10453 (2005).
- [4] Sajedeheh Manzeli, Dmitry Ovchinnikov, Diego Pasquier, Oleg V. Yazyev, and Andras Kis, "2d transition metal dichalcogenides," *Nat. Rev. Mater.* **2**, 17033 (2017).
- [5] C. L. Kane and E. J. Mele, *Phys. Rev. Lett.* **95**, 226801 (2005).
- [6] C. L. Kane and E. J. Mele, *Phys. Rev. Lett.* **95**, 146802 (2005).
- [7] A. Bansil, Hsin Lin, and Tanmoy Das, "Colloquium: Topological band theory," *Rev. Mod. Phys.* **88**, 021004 (2016).
- [8] M. Z. Hasan and C. L. Kane, "Colloquium: Topological insulators," *Rev. Mod. Phys.* **82**, 3045–3067 (2010).
- [9] B. Andrei Bernevig and Shou-Cheng Zhang, "Quantum spin hall effect," *Phys. Rev. Lett.* **96**, 106802 (2006).
- [10] B. Andrei Bernevig, Taylor L. Hughes, and Shou-Cheng Zhang, *Science* **314**, 1757–1761 (2006).
- [11] Bahadur Singh, Hsin Lin, R. Prasad, and A. Bansil, "Topological phase transition and two-dimensional topological insulators in ge-based thin films," *Phys. Rev. B* **88**, 195147 (2013).
- [12] Antimo Marrazzo, Marco Gibertini, Davide Campi, Nicolas Mounet, and Nicola Marzari, "Prediction of a large-gap and switchable kane-mele quantum spin hall insulator," *Phys. Rev. Lett.* **120**, 117701 (2018).
- [13] Xiaofeng Qian, Junwei Liu, Liang Fu, and Ju Li, *Science* **346**, 1344–1347 (2014).
- [14] Yong Xu, Binghai Yan, Hai-Jun Zhang, Jing Wang, Gang Xu, Peizhe Tang, Wenhui Duan, and Shou-Cheng Zhang, *Phys. Rev. Lett.* **111**, 136804 (2013).
- [15] Chaoxing Liu, Taylor L. Hughes, Xiao-Liang Qi, Kang Wang, and Shou-Cheng Zhang, *Phys. Rev. Lett.* **100**, 236601 (2008).
- [16] Markus KÄ¶nig, Steffen Wiedmann, Christoph BrÄ¶ene, Andreas Roth, Hartmut Buhmann, Laurens W. Molenkamp, Xiao-Liang Qi, and Shou-Cheng Zhang, *Science* **318**, 766–770 (2007).
- [17] Ivan Knez, Rui-Rui Du, and Gerard Sullivan, *Phys. Rev.*

- Lett.* **107**, 136603 (2011).
- [18] Shujie Tang, Chaofan Zhang, Dillon Wong, Zahra Pedramrazi, Hsin-Zon Tsai, Chunjing Jia, Brian Moritz, Martin Claassen, Hyejin Ryu, Salman Kahn, *et al.*, *Nat. Phys.* **13**, 683–687 (2017).
- [19] Konrád Kandrai, Péter Vancsó, Gergő Kukucska, János Koltai, György Baranka, Ákos Hoffmann, Áron Pekker, Katalin Kamarás, Zsolt E. Horváth, Anna Vymazalová, Levente Tapasztó, and Péter Nemes-Incze, “Signature of large-gap quantum spin hall state in the layered mineral jacutingaite,” *Nano Lett.* **20**, 5207–5213 (2020).
- [20] Nana Shumiya, Md Shafayat Hossain, Jia-Xin Yin, Zhiwei Wang, Maksim Litskevich, Chiho Yoon, Yongkai Li, Ying Yang, Yu-Xiao Jiang, Guangming Cheng, Yen-Chuan Lin, Qi Zhang, Zi-Jia Cheng, Tyler A. Cochran, Daniel Multer, Xian P. Yang, Brian Casas, Tay-Rong Chang, Titus Neupert, Zhujun Yuan, Shuang Jia, Hsin Lin, Nan Yao, Luis Balicas, Fan Zhang, Yugui Yao, and M. Zahid Hasan, “Room-temperature quantum spin hall edge state in a higher-order topological insulator Bi_4Br_4 ,” [Arxiv.2110.05718](https://arxiv.org/abs/2110.05718) (2022), [10.48550/arXiv.2110.05718](https://arxiv.org/abs/2110.05718).
- [21] Zaiyao Fei, Tauno Palomaki, Sanfeng Wu, Wenjin Zhao, Xinghan Cai, Bosong Sun, Paul Nguyen, Joseph Finney, Xiaodong Xu, and David H. Cobden, “Edge conduction in monolayer wTe_2 ,” *Nat. Phys.* **13**, 677–682 (2017).
- [22] Sanfeng Wu, Valla Fatemi, Quinn D. Gibson, Kenji Watanabe, Takashi Taniguchi, Robert J. Cava, and Pablo Jarillo-Herrero, *Science* **359**, 76–79 (2018).
- [23] Hsin Lin, R. S. Markiewicz, L. A. Wray, L. Fu, M. Z. Hasan, and A. Bansil, “Single-dirac-cone topological surface states in the tlbise_2 class of topological semiconductors,” *Phys. Rev. Lett.* **105**, 036404 (2010).
- [24] Yan-Fang Zhang, Jinbo Pan, Huta Banjade, Jie Yu, Hsin Lin, Arun Bansil, Shixuan Du, and Qimin Yan, *Nano Res.* **14**, 584–589 (2021).
- [25] Zhen-Yu Jia, Ye-Heng Song, Xiang-Bing Li, Kejing Ran, Pengchao Lu, Hui-Jun Zheng, Xin-Yang Zhu, Zhi-Qiang Shi, Jian Sun, Jinsheng Wen, Dingyu Xing, and Shao-Chun Li, *Phys. Rev. B* **96**, 041108 (2017).
- [26] Zhuojun Li, Yekai Song, and Shujie Tang, *J. Phys. Condens. Matter* **32**, 333001 (2020).
- [27] Y. Cao, A. Mishchenko, G. L. Yu, E. Khestanova, A. P. Rooney, E. Prestat, A. V. Kretinin, P. Blake, M. B. Shalom, C. Woods, J. Chapman, G. Balakrishnan, I. V. Grigorieva, K. S. Novoselov, B. A. Piot, M. Potemski, K. Watanabe, T. Taniguchi, S. J. Haigh, A. K. Geim, and R. V. Gorbachev, *Nano Lett.* **15**, 4914–4921 (2015).
- [28] Lin Wang, Ignacio Gutiérrez-Lezama, Céline Barreteau, Nicolas Ubrig, Enrico Giannini, and Alberto F Morpurgo, *Nat. Commun.* **6**, 1–7 (2015).
- [29] Fan Ye, Jaesung Lee, Jin Hu, Zhiqiang Mao, Jiang Wei, and Philip X.-L. Feng, *Small* **12**, 5802–5808.
- [30] K. S. Novoselov, A. Mishchenko, A. Carvalho, and A. H. Castro Neto, “2d materials and van der waals heterostructures,” *Science* **353**, aac9439 (2016).
- [31] Kostya S Novoselov, “Discovery of 2D van der Waals layered MoSi_2N_4 family,” *National Science Review* **7**, 1842–1844 (2020).
- [32] Yi-Lun Hong, Zhibo Liu, Lei Wang, Tianya Zhou, Wei Ma, Chuan Xu, Shun Feng, Long Chen, Mao-Lin Chen, Dong-Ming Sun, *et al.*, *Science* **369**, 670–674 (2020).
- [33] Rajibul Islam, Barun Ghosh, Carmine Autieri, Sugata Chowdhury, Arun Bansil, Amit Agarwal, and Bahadur Singh, *Phys. Rev. B* **104**, L201112 (2021).
- [34] Chen Yang, Zhigang Song, Xiaotian Sun, and Jing Lu, *Phys. Rev. B* **103**, 035308 (2021).
- [35] Si Li, Weikang Wu, Xiaolong Feng, Shan Guan, Wanxiang Feng, Yugui Yao, and Shengyuan A. Yang, *Phys. Rev. B* **102**, 235435 (2020).
- [36] Xiangyu Feng, Xilong Xu, Zhonglin He, Rui Peng, Ying Dai, Baibiao Huang, and Yandong Ma, *Phys. Rev. B* **104**, 075421 (2021).
- [37] Simone Bertolazzi, Jacopo Brivio, and Andras Kis, *ACS nano* **5**, 9703–9709 (2011).
- [38] Yongqing Cai, Gang Zhang, and Yong-Wei Zhang, *J. Am. Chem. Soc* **136**, 6269–6275 (2014).
- [39] Rajibul Islam, Barun Ghosh, Giuseppe Cuono, Alexander Lau, Wojciech Brzezicki, Arun Bansil, Amit Agarwal, Bahadur Singh, Tomasz Dietl, and Carmine Autieri, “Topological states in superlattices of hgte class of materials for engineering three-dimensional flat bands,” *Phys. Rev. Research* **4**, 023114 (2022).
- [40] L. Matthes, S. Kufner, J. Furthmüller, and F. Bechstedt, “Intrinsic spin hall conductivity in one-, two-, and three-dimensional trivial and topological systems,” *Phys. Rev. B* **94**, 085410 (2016).
- [41] Yan Sun, Yang Zhang, Claudia Felser, and Binghai Yan, “Strong intrinsic spin hall effect in the taas family of weyl semimetals,” *Phys. Rev. Lett.* **117**, 146403 (2016).
- [42] Ruiqi Zhang, Cheng-Yi Huang, Jamin Kidd, Robert S. Markiewicz, Hsin Lin, Arun Bansil, Bahadur Singh, and Jianwei Sun, “Weyl semimetal in the rare-earth hexaboride family supporting a pseudonodal surface and a giant anomalous hall effect,” *Phys. Rev. B* **105**, 165140 (2022).
- [43] Jiaqi Zhou, Junfeng Qiao, Arnaud Bournel, and Weisheng Zhao, “Intrinsic spin hall conductivity of the semimetals mTe_2 and wTe_2 ,” *Phys. Rev. B* **99**, 060408 (2019).
- [44] Junfeng Qiao, Jiaqi Zhou, Zhe Yuan, and Weisheng Zhao, “Calculation of intrinsic spin hall conductivity by wannier interpolation,” *Phys. Rev. B* **98**, 214402 (2018).
- [45] Filipe Matusalem, Marcelo Marques, Lara K. Teles, Lars Matthes, Jürgen Furthmüller, and Friedhelm Bechstedt, “Quantization of spin hall conductivity in two-dimensional topological insulators versus symmetry and spin-orbit interaction,” *Phys. Rev. B* **100**, 245430 (2019).
- [46] P. Hohenberg and W. Kohn, “Inhomogeneous electron gas,” *Phys. Rev.* **136**, B864–B871 (1964).
- [47] G. Kresse and J. Furthmüller, *Phys. Rev. B* **54**, 11169–11186 (1996).
- [48] John P. Perdew, Kieron Burke, and Matthias Ernzerhof, *Phys. Rev. Lett.* **77**, 3865–3868 (1996).
- [49] Jochen Heyd, Gustavo E. Scuseria, and Matthias Ernzerhof, “Hybrid functionals based on a screened coulomb potential,” *J. Chem. Phys.* **118**, 8207–8215 (2003).
- [50] Atsushi Togo and Isao Tanaka, *Scripta Materialia* **108**, 1–5 (2015).
- [51] Robert N. Barnett and Uzi Landman, *Phys. Rev. B* **48**, 2081–2097 (1993).
- [52] Arash A. Mostofi, Jonathan R. Yates, Young-Su Lee, Ivo Souza, David Vanderbilt, and Nicola Marzari, *Computer Physics Communications* **178**, 685–699 (2008).
- [53] QuanSheng Wu, ShengNan Zhang, Hai-Feng Song, Matthias Troyer, and Alexey A. Soluyanov, *Computer Physics Communications* **224**, 405–416 (2018).
- [54] M P Lopez Sancho, J M Lopez Sancho, J M L Sancho, and J Rubio, *Journal of Physics F: Metal Physics* **15**,

851–858 (1985).